Eur. J. Mineral., 35, 873–890, 2023
https://doi.org/10.5194/ejm-35-873-2023

European Journal of Mineralogy
Open Access

Vibrational properties of OH groups associated with divalent cations in corundum (α-Al_2O_3)

Michael C. Jollands[1], Shiyun Jin[2], Martial Curti[3], Maxime Guillaumet[4], Keevin Béneut[4], Paola Giura[4], and Etienne Balan[4]

[1]Gemological Institute of America, 50 W 47th Street, New York, NY 10036, USA
[2]Gemological Institute of America, 5355 Armada Drive, Carlsbad, CA 92008, USA
[3]Bellerophon Gemlab SAS, 16 Place Vendôme, Paris 75001, France
[4]Sorbonne Université, CNRS, MNHN, IRD, Institut de Minéralogie, de Physique des Matériaux et de Cosmochimie (IMPMC), 4 place Jussieu, 75252 Paris CEDEX 05, France

Correspondence: Etienne Balan (etienne.balan@sorbonne-universite.fr)

Received: 5 May 2023 – Revised: 29 August 2023 – Accepted: 4 September 2023 – Published: 19 October 2023

Abstract. The infrared spectra of synthetic corundum (α-Al_2O_3) samples either doped directly with divalent cations (Mg^{2+}) or containing divalent cations formed by reduction of trivalent cations in H_2 gas (Co^{2+}, Ni^{2+}) may display broad OH stretching bands at $\sim 3000\,cm^{-1}$ due to the structural incorporation of trace amounts of hydrogen. Experimental spectra recorded from some natural sapphires display a similar absorption band associated with a dominant absorption at $3161\,cm^{-1}$, and some beryllium-diffused corundum crystals show a band at $3060\,cm^{-1}$. All of these also display smaller and generally narrower bands between 1900 and $2700\,cm^{-1}$, whose natures are poorly defined. In this work, the atomic-scale structure, relative stability and infrared spectroscopic properties of a series of OH defects in corundum (α-Al_2O_3) are theoretically investigated at the density-functional-theory level. The investigated defects consist of interstitial H^+ ions forming OH groups and compensating for the charge imbalance related to the presence of divalent cations (Be^{2+}, Mg^{2+}, Cr^{2+}, Mn^{2+}, Fe^{2+}, Co^{2+}, Ni^{2+}) substituted for Al^{3+} at nearby octahedral sites. Bands occurring at $\sim 3000\,cm^{-1}$ in experimental spectra are assigned to the OH stretching modes of some of these defects, with bands observed around 1900 and $2700\,cm^{-1}$ being assigned to overtones of corresponding OH bending modes. The results also support the assignment of the so-called "$3161\,cm^{-1}$ series", observed in experimental spectra of some rubies and yellow sapphires, to structural OH groups in association with Fe^{2+} ions, rather than Si^{4+}, as has been previously proposed. These inferences are also supported by analysis of correlations between band areas in experimental infrared spectra extracted from a database of corundum gemstones. A qualitative explanation relating the anomalous intensity and the polarisation properties of the OH bending overtone bands to the electrical anharmonicity of OH groups involved in medium-strength H bonds is proposed.

1 Introduction

The infrared spectra of synthetic or natural corundum (α-Al_2O_3) samples display a significant variability in the OH stretching region which relates to their growth conditions, trace element contents and thermal history. While some spectra recorded from natural samples suggest the presence of hydrous solid inclusions, such as kaolinite or diaspore, OH stretching bands related to trace concentrations of OH groups incorporated at structural crystal sites are also observed (e.g. Beran and Rossman, 2006). These OH groups result from the bonding of H^+ ions to oxygen anions, ensuring an electrostatic charge compensation for Al^{3+} vacancies or for Al^{3+} substitution by lower-valency cations.

The presence of OH groups associated with Al vacancies (Moon and Phillips, 1991, 1994; Balan, 2020) leads to well-resolved bands between 3150 and $3400\,cm^{-1}$, most frequently at 3309, 3232 and $3185\,cm^{-1}$, with a polarisation almost parallel to the (001) plane. These bands correspond

to the so-called "3309 cm^{-1} series" (e.g. Soonthorntantikul et al., 2019) and can be observed in synthetic samples (e.g. Eigenmann and Günthard, 1971; Volynets et al., 1972; Beran, 1991; Ramírez et al., 2004) or natural samples (e.g. Beran and Rossman, 2006; Soonthorntantikul et al., 2019).

Turning to the presence of OH groups associated with divalent cations, spectra of synthetic samples doped with Co^{3+} or Ni^{3+} and then reduced to Co^{2+} and Ni^{2+}, respectively, through annealing in a H_2 atmosphere at $> 800\,°C$ display relatively broad OH stretching bands extending from ~ 2700 to $\sim 3300\,cm^{-1}$ (Müller and Günthard, 1966; Eigenmann and Günthard, 1971; Blum et al., 1973). These spectra also display several narrower bands between 1900 and 2700 cm^{-1} (e.g. Müller and Günthard, 1966). Similar infrared spectra are recorded from synthetic corundum samples doped with Mg with a main broad band at $\sim 3000\,cm^{-1}$ and weaker and narrower bands at 2030, 2140, 2254, 2416, 2462 and 2628 cm^{-1} (Fukatsu et al., 2003). The main broad band has a dominant polarisation in the direction perpendicular to the (001) plane (Volynets et al., 1972; Ramírez et al., 1997; Fukatsu et al., 2003) and most of the low-wavenumber bands have similar pleochroism (Fukatsu et al., 2003). Spectra very close to those of the synthetic Mg-bearing samples are observed in some natural untreated sapphires and in some "Punsiri" heat-treated sapphires (Bonnet and Fritsch, 2012; Sangsawong et al., 2016; Hummel, 2019). The spectra of Be-diffused corundum samples can also display a broad band at 3060 cm^{-1} as well as a band at 2490 cm^{-1} (Balmer and Krzemnicki, 2015; Jollands and Balan, 2022).

The nature of the bands observed between 1900 and 2700 cm^{-1} in corundum samples containing divalent cations is undefined. Some of these bands are often weak and may overlap with those associated with CO_2 (2250 to 2400 cm^{-1}), which are ubiquitous in routine infrared spectroscopy analyses. There is therefore a possibility that their presence may be underreported in the literature. High-temperature diffusion experiments suggest that they are related to hydrogen-bearing species (e.g. Müller and Günthard, 1966). The low natural abundance of deuterium (D), as well as results from deuterium diffusion experiments (e.g. Müller and Günthard, 1966; Fukatsu et al., 2003), rules out an assignment of these low-frequency bands to OD stretching vibrations. Although their frequency could match the fundamental frequency of relatively covalent X–H bonds, such as Be–H, as proposed by Jollands and Balan (2022) for Be-diffused samples, their occurrence in high-temperature synthetic samples with controlled chemical composition, as well as their presence in natural samples with highly variable compositions, challenges this hypothesis. Alternatively, these bands could correspond to overtones of lower-frequency vibrational modes. Unfortunately, the corresponding fundamental modes cannot be observed in routine gemstone analysis because of the strong absorption of corundum below 2000 cm^{-1}, generally leading to the saturation of spectra. In addition, the overtone transitions are forbidden in the harmonic approximation and their intensities can be several orders of magnitude weaker than those of their fundamental counterparts. For this reason, overtones of OH bending modes of hydrous defects are usually not expected to be observed in standard infrared spectroscopic analysis.

Additionally, the experimental infrared spectra of some natural corundum display a dominant band at 3161–3164 cm^{-1}, a broad feature at $\sim 3075\,cm^{-1}$, and two narrow bands at 3242 and 3355 cm^{-1} (Smith and Van der Bogert, 2006; Schwarz et al., 2008; Choudhary and Vijay, 2018; Hummel 2019). Low-frequency bands have also been reported at 2420 and 2460 cm^{-1}. As the 3161 cm^{-1} band disappears for samples heated above 900 °C in air, presumably associated with out-diffusion of hydrogen (Atikarnsakul and Emmett, 2021), its presence may be indicative of unheated sapphires (Choudhary and Vijay, 2018). Its nature is however unclear. It has been related to the presence of Si^{4+} in corundum samples (Volynets et al., 1972), to the association of hydrogen with Mg^{2+} cations (Smith and Van der Bogert, 2006), and to inclusion of other phases such as goethite or epidote (Balmer et al., 2006). Choudhary and Vijay (2018) related this band to the narrow band observed at 3163 cm^{-1} in experimental spectra recorded from synthetic Verneuil samples, but in this case, the low-frequency bands are lacking.

Approaches based on the density-functional theory (DFT) can be used to establish theoretical relations between the observed infrared spectroscopic signals and atomic-scale models of hydrous defects in minerals (e.g. Jollands et al., 2020, for quartz; Balan, 2020, and Jollands and Balan, 2022, for corundum). Here, the atomic-scale structures of defective corundum models associating H atoms with substituted divalent cations are theoretically determined and their calculated spectroscopic properties are compared to available experimental spectra recorded from both synthetic and natural corundum. These investigations are completed by a statistical analysis of spectra extracted from a database of infrared spectra recorded from corundum gemstones. By coupling theoretical and experimental data, the results support the assignment of the low-frequency bands to overtones of OH bending modes and provide interpretations for major bands observed in the spectra of synthetic or natural corundum samples containing divalent cations.

2 Methods

2.1 Theoretical modelling

The properties of OH defects in corundum were theoretically investigated using the same approach and numerical parameters as in Balan et al. (2020) and Jollands and Balan (2022). Briefly, the defect modelling was performed within the DFT framework using the generalised gradient approximation (GGA) to the exchange–correlation functional as proposed by Perdew, Burke and Ernzerhof (PBE functional;

Perdew et al., 1996). The modelling scheme used periodic boundary conditions and a plane-wave basis set as implemented in the PWscf code of the Quantum Espresso package (Giannozzi et al., 2009; http://www.quantum-espresso.org, last access: 6 October 2023). Ionic cores were described using optimised norm-conserving Vanderbilt (SG15 ONCV) pseudopotentials (Hamann, 2013; Schlipf and Gygi, 2015) with a plane-wave energy cutoff of 80 Ry.

Structural properties of OH-bearing defects were determined using $2 \times 2 \times 1$ corundum supercells (120 atoms) with Brillouin zone sampling restricted to the Γ point. The relaxation of atomic internal coordinates was performed until the residual forces were $< 10^{-4}$ Ry au^{-1}. Unit-cell parameters of pure corundum optimised at zero pressure ($a = b =$ 4.80 Å, $c = 13.08$ Å) were used without further relaxation to produce the OH-bearing supercells. For models with paramagnetic cations, spin-polarised calculations have been performed, imposing the spin state of isolated ions onto the supercell and assuming a high-spin state for Cr^{2+}, Mn^{2+}, Fe^{2+} and Co^{2+} cations. The vibrational modes at the Brillouin zone centre (Γ point), the Born effective charge tensors and the electronic dielectric tensor were then calculated using the linear response theory (Baroni et al., 2001) as implemented in the PHonon code (Giannozzi et al., 2009; http://www.quantum-espresso.org, last access: 6 October 2023). As the OH bending modes are also relevant for the present study, the partial Hessian technique, which provides accurate results for the OH stretching mode, was not used and full dynamical matrices (leading to 363 modes for each H-bearing model) were calculated.

The angle between the mode-effective charge vector and the [001] direction (Θ_{spectro}, Table 1) is the quantity which can be experimentally determined from the variation in the IR absorption intensity as a function the IR light polarisation (e.g. Libowitzky and Beran, 2006). The mode-effective charge vector is proportional to the polarisation induced by the atomic displacements in the related vibrational mode and is defined by (Gonze and Lee, 1997)

$$Z^*_{m,\alpha} = \frac{\sum_{\tau\beta} Z^*_{\tau,\alpha\beta} U_m(\tau\beta)}{\sqrt{\sum_{\tau\beta} U_m(\tau\beta)^* U_m(\tau\beta)}},$$

where $Z^*_{\tau,\alpha\beta}$ is the Born effective charge tensor which describes the polarisation induced in the Cartesian direction α by the displacement of atom τ in the Cartesian direction β and $U_{\text{m}}(\tau\beta)$ is the displacement coordinate along β of atom τ of mode m. $U_{\text{m}}(\tau\beta)$ is normalised such that $\sum_{\tau\beta} M_\tau U_m(\tau\beta)^* U_m(\tau\beta) = \delta_{nm}$, where M_τ is the mass of atom τ and $\delta_{mn} = 1$ if $m = n$ and $\delta_{mn} = 0$ otherwise. Due to the potential anisotropy of the Born effective charge tensors, the Θ_{spectro} angle can differ from the Θ_{stretch} angle defined between the stretching direction of the OH group and the [001] direction (Table 1).

2.2 Infrared spectroscopy

To complement the DFT modelling, Fourier-transform infrared (FTIR) spectra were manually selected from a large database of unpolarised experimental spectra of faceted gemstones recorded at laboratories of the Gemological Institute of America (GIA). In general, these are recorded using Thermo iS50 spectrometers equipped with MCT detectors, using an instrumental resolution of 2 cm^{-1} and ≥ 32 scans. Three types of spectrum were extracted. The first set comprised 250 spectra of natural samples showing a clear band at 3161 cm^{-1}, without any broad band at around 3000 cm^{-1} or bands from the "3309 cm^{-1} series", which is usually characterised by a main band centred at 3309 cm^{-1}. The second set is a compilation of spectra showing a double peak at 3015 and 2970 cm^{-1}, recorded from synthetic corundum crystals with relatively high Ni concentrations (> 7 wt ppm). Such crystals are rarely submitted for examination, and trace element data are generally unnecessary to confirm their synthetic nature. As a result, only 14 such spectra were available. The third set corresponds to spectra showing the broad band observed in Mg-doped synthetic crystals, with a doublet at 3207 and 2991 cm^{-1}, with broad tails on this main band often extending to > 3300 and < 2800 cm^{-1}. Such spectra can be observed in synthetic corundum, as well as natural and Punsiri-treated crystals. All spectra were then baseline-corrected using a concave-rubber-band method and then fitted with Gaussian peak-shape functions, with a different series of functions used for the three types of spectrum. The integrated areas of the bands were compiled for each spectrum. No thickness correction was made; therefore all integrated absorbance is arbitrary. The aim of this exercise is to determine which bands show correlations with one another, which is useful for supporting or refuting assignation of different bands to the same defect, or at least the same class of defect. Unfortunately, it was not possible to identify experimental FTIR spectra of hydrous defects in corundum related to Mn^{2+} or Cr^{2+} in the GIA database or in the literature.

Finally, transmission FTIR spectra were recorded from a 3.3 mm thick slab of a natural yellow sapphire (YS-1) from Sri Lanka showing the 3161 cm^{-1} band, for which polarisation information was lacking. The spectra were obtained for polarisation directions roughly parallel or perpendicular to the [001] direction with an instrumental resolution of 4 cm^{-1}, using a Nicolet 6700 FTIR spectrometer and Continuμm microscope, set with an EverGlo source, KBr beam splitter and MCT detector.

Table 1. Theoretical structural and harmonic vibrational properties of models associating one interstitial H^+ with substitutions at nearby octahedral sites. Each substituted model displays four configurations. The table columns are as follows. "Model" gives the substituting cation name and specifies the configuration. Sites 1 to 4 describe site occupancy in the related configuration, as shown in Fig. 1. "Rel. energy" is the energy of each configuration defined relative to the most stable configuration with the same stoichiometry. "d(OH)" is the O–H distance. "ω_{OH}" is the wavenumber of the OH stretching vibration. "$\Theta_{stretch}$" and "$\Theta_{spectro}$" are the angles of the stretching displacement direction and of the induced polarisation vector, respectively, with respect to the [001] direction. "K_{int}" is the absorption coefficient for the configuration. "δ_{OH}" and "γ_{OH}" are the wavenumbers of the δ and γ bending modes, respectively.

Model	Site 1	Site 2	Site 3	Site 4	Rel. energy ($kJ\,mol^{-1}$)	d(OH) (Å)	ω_{OH} (cm^{-1})	$\Theta_{stretch}$ (°)	$\Theta_{spectro}$ (°)	K_{int} ($L\,mol^{-1}\,cm^{-2}$)	δ_{OH} (cm^{-1})	$2\times\delta_{OH}$ (cm^{-1})	γ_{OH} (cm^{-1})	$2\times\gamma_{OH}$ (cm^{-1})
$(H^+)_i$	Al	Al	Al	Al	–	1.0073	2995	37	36	188 000	1277	2554	956	1912
$(Be)_{Al}$–OH_{in}	Be^{2+}	Al	Al	Al	–	0.9988	3096	33	36	261 000	1257	2514	1020	2040
Mg_1	Mg^{2+}	Al	Al	Al	0	1.0063	2990	34	38	225 000	1331	2663	1005	2010
Mg_2	Al	Mg^{2+}	Al	Al	13	1.0034	3039	35	33	192 000	1302	2605	893	1786
Mg_3	Al	Al	Mg^{2+}	Al	17	0.9952	3216	46	40	111 000	1201	2401	896	1793
Mg_4	Al	Al	Al	Mg^{2+}	3	0.9961	3196	36	34	131 000	1209	2419	876	1753
Cr_1	Cr^{2+}	Al	Al	Al	8	1.0013	3060	30	35	135 000	1171	2342	948	1897
Cr_2	Al	Cr^{2+}	Al	Al	30	1.0051	2969	37	36	220 000	1321	2643	904	1807
Cr_3	Al	Al	Cr^{2+}	Al	17	1.0048	2957	64	75	137 000	1165	2331	886	1771
Cr_4	Al	Al	Al	Cr^{2+}	0	1.0012	3109	37	31	95 000	1122	2243	901	1803
Mn_1	Mn^{2+}	Al	Al	Al	0	0.9993	3101	32	37	162 000	1236	2472	969	1939
Mn_2	Al	Mn^{2+}	Al	Al	27	1.0082	2931	35	37	236 000	1314	2628	918	1837
Mn_3	Al	Al	Mn^{2+}	Al	43	0.9958	3197	50	41	76 000	1139	2278	879	1759
Mn_4	Al	Al	Al	Mn^{2+}	3	0.9914	3295	35	26	91 000	1152	2304	833	1667
Fe_1	Fe^{2+}	Al	Al	Al	0	1.0047	3020	34	36	153 000	1210	2420	944	1888
Fe_2	Al	Fe^{2+}	Al	Al	18	1.0048	3002	34	36	195 000	1311	2621	903	1805
Fe_3	Al	Al	Fe^{2+}	Al	12	1.0111	2920	54	86	79 000	1090	2181	883	1766
Fe_4	Al	Al	Al	Fe^{2+}	5	0.9942	3231	36	33	119 000	1176	2352	847	1695
Co_1	Co^{2+}	Al	Al	Al	0	1.0035	3034	33	37	160 000	1238	2475	958	1917
Co_2	Al	Co^{2+}	Al	Al	19	1.0044	3011	34	36	143 000	1303	2606	895	1790
Co_3	Al	Al	Co^{2+}	Al	14	0.9979	3171	55	65	55 000	1050	2100	862	1724
Co_4	Al	Al	Al	Co^{2+}	7	0.9951	3217	36	32	125 000	1191	2381	852	1703
Ni_1	Ni^{2+}	Al	Al	Al	0	1.0065	2997	33	37	152 000	1219	2438	969	1939
Ni_2	Al	Ni^{2+}	Al	Al	9	1.0031	3043	34	38	174 000	1300	2601	896	1793
Ni_3	Al	Al	Ni^{2+}	Al	0	0.9947	3239	52	46	66 000	1034	2067	871	1743
Ni_4	Al	Al	Al	Ni^{2+}	7	0.9991	3140	36	34	153 000	1211	2423	886	1772

3 Results and discussion

3.1 General properties of interstitial H^+ in corundum

Hydrous defects comprising a cationic substitution, such as Mg^{2+} for Al^{3+}, associated with an interstitial H^+ (Fig. 1), are closely related to the $(H^+)_i$ model previously investigated by Zhang et al. (2014), T-Thienprasert et al. (2017) and Balan (2020). In this positively charged model, the OH group resulting from the bonding of the H atom to an oxygen atom of the corundum structure is coordinated to four Al atoms. The theoretical model of Balan (2020) displays an OH bond length of 1.0073 Å and an OH stretching frequency of 2994 cm^{-1}. Two OH bending modes, denoted δ and γ, are predicted at 1277 and 956 cm^{-1}, respectively (Table 1; eigendisplacements are reported as electronic files in the Supplement). These bending modes correspond to a hydrogen displacement dominantly parallel (δ mode) or perpendicular (γ mode) to the [001] direction. Note that OH vibrational modes of crystals involving a displacement of the H atom in a direction perpendicular to the OH bond are referred to as libration modes in basic hydroxides, such as LiOH or NaOH, and as bending modes in systems with more covalent bonds, such as Al hydroxides (Ryskin, 1974). Bending modes usually correspond to higher vibrational frequencies than libration modes. For the three vibrational modes, the norm of the H-atom displacement vector accounts for more than 99 % of the norm of the full atomic displacement vectors. Therefore, the vibrational properties of the OH groups can be qualitatively discussed by considering only the hydrogen displacement (whilst the other atoms interacting with the hydrogen must be considered for a quantitative treatment). The H atom also contributes to lower-frequency modes due to the coupling of its displacements with the corundum vibrational modes involving the Al and O atoms. For most of these modes, the H displacement is not dominant and accounts for less than 50 % of the norm of the full atomic displacement vectors. One theoretical mode at 764 cm^{-1} displays a more significant contribution of the hydrogen displacement (63 %), with a displacement pattern similar to that of the

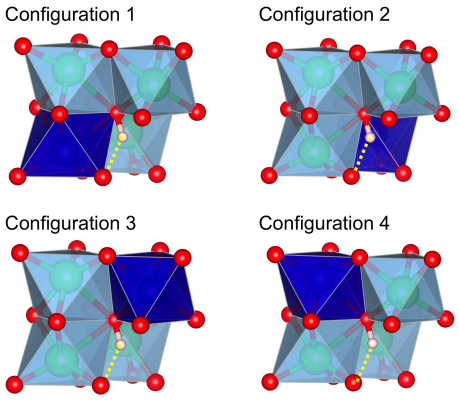

Figure 1. Configurations of interstitial H^+ associated with a divalent cation in corundum. The configurations differ by the occupancy of one of the four octahedral sites (deep blue) surrounding the OH group. The OH group forms a medium-strength H bond (dotted yellow line) with an oxygen anion of the structurally vacant octahedral site. Red sphere: oxygen atom; light-pink sphere: hydrogen atom; green sphere: aluminium.

γ bending mode (theoretical eigendisplacements and animation files are provided in the Supplement).

For one cationic substitution, four non-equivalent defect configurations display a M^{2+}–OH bond (Table 1). They differ by the respective position of the OH group and substituted Al site (Fig. 1). All of the configurations are electrostatically neutral. In configurations 1 and 4, the H atom is bonded to an oxygen atom of the small oxygen triangle shared by the substituted octahedral site and the neighbouring Al-occupied site. The two configurations differ by the orientation of the OH bond, which points along the edge of the substituted site in configuration 1 and in the opposite direction in configuration 4. In configurations 2 and 3, the hydrogen atom is connected to the large basal oxygen triangle between the substituted site and the neighbouring structurally vacant octahedral site. The OH bond is in a lateral position with respect to the face of the substituted site in configuration 3 and points in the opposite direction in configuration 2 (Fig. 1). The relative energy of the configurations (Table 1) suggests that H being bonded to an oxygen of the small triangle (configurations 1 and 4) is favoured relative to bonding on the large oxygen triangle (configurations 2 and 3), except in the Ni-bearing configurations, which display a smaller variation range in their total energy. The conversion between configurations 1 and 2 corresponds to a H^+ exchange between two oxygen anions belonging to the same structurally vacant octahedral site. This suggests that this conversion is very easy, which implies that the less stable configuration 2 is not expected to occur at significant concentrations at room temperature.

The orientation and length of the OH groups in the whole series of models are generally close to those determined for the $(H^+)_i$ model, with theoretical bond lengths between 0.99 and 1.015 Å. Variations in the OH bond length are correlated

Table 2. Vibrational modes of the $(H^+)_i$ and Mg, Fe, Co and Ni models at frequencies above 700 cm^{-1} and displaying a coupled contribution of the hydrogen atom accounting for more than 60 % of the norm of the atomic displacement vector. Some of these modes are expected to lead to the second overtone bands observed between 2100 and 2400 cm^{-1} in the corresponding spectra.

Model	Frequency (cm^{-1})	Hydrogen contribution (%)
$(H^+)_i$	764	63
Mg_2	763	71
Mg_3	760	71
Mg_4	755	71
Fe_2	763	65
Fe_3	760	78
Fe_4	798	62
	740	62
	707	66
Co_2	762	67
Co_3	798	61
	756	79
Co_4	751	63
	707	62
Ni_2	761	67
Ni_3	756	77
Ni_4	756	73

to variations in the OH stretching frequency (Fig. 2a), as previously observed (e.g. Jollands et al., 2020; Balan, 2020). Most of the theoretical OH stretching frequencies range between 2900 and 3200 cm^{-1}, corresponding to the range expected for OH groups involved in medium-strength H bonds (Nibbering et al., 2007). The theoretical bending frequencies occur between 1000 and 1400 cm^{-1} (δ mode) and between 800 and 1100 cm^{-1} (γ mode). They broadly decrease as a function of the stretching frequencies of OH groups (Fig. 2b). Interestingly, some of the configurations also display theoretical vibrational modes at lower frequency involving a significant contribution (up to 79 %) of the hydrogen displacement coupled to a vibrational mode of the corundum host, similar to that observed in the $(H^+)_i$ model (Table 2). It is noteworthy that this type of mode does not appear in all the configurations and should be highly sensitive to the respective vibrational properties of the molecular impurity and of the crystal host.

The theoretical absorption coefficient of the stretching modes (Fig. 2c, Table 1) roughly decreases as a function of the stretching frequency, which is consistent with the general properties of OH groups in minerals and crystalline solids, as determined from experimentation (Libowitzky and Rossman, 1997) or theory (Balan et al., 2008). This variation in the theoretical absorption coefficient is related to the variation in the magnitude of the Born effective charge tensor of hydro-

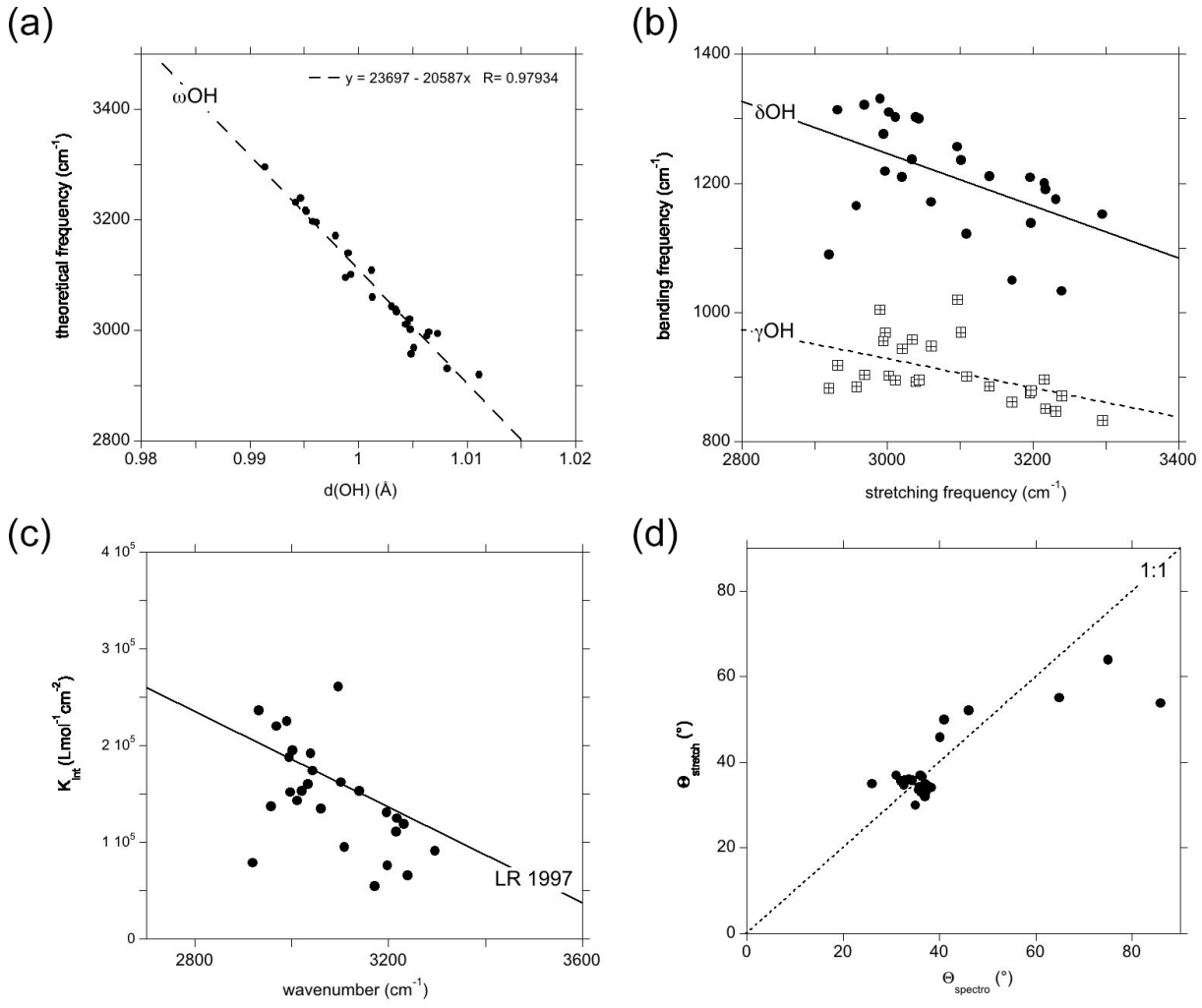

Figure 2. Theoretical vibrational properties of the hydrous defects in corundum (Table 1). **(a)** Relation between the OH stretching frequency and the OH bond length. **(b)** Frequency of the OH bending modes (filled circles: δ modes; open squares: γ modes) reported as a function of the corresponding stretching mode. **(c)** Theoretical infrared absorption coefficient of the OH stretching mode as a function of the corresponding theoretical frequency. The straight line (LR 1997) corresponds to the Libowitzky and Rossman (1997) experimental calibration ($K_{\mathrm{int}} = 246.6\,(3753 - \nu_{\mathrm{OH}})$), where K_{int} is the absorption coefficient of the OH stretching band in units of cm^{-2} per mol $\mathrm{H_2O\,L^{-1}}$ and ν_{OH} the observed stretching frequency in reciprocal centimetres (cm^{-1}). **(d)** Comparison of the theoretical polarisation angle inferred from the spectroscopic properties of the models to that corresponding to the stretching coordinates.

gen along the H-displacement direction, which increases as a function of the H-bond strength (Balan et al., 2008). One of the configurations (Fe_3 configuration, Table 1) however combines a relatively low theoretical absorption coefficient and low theoretical stretching frequency (Fig. 2c). In this configuration, the substituting Fe^{2+} cation occupies a lateral position with respect to the OH group (Fig. 1).

For most of the models, the theoretical infrared absorption related to stretching modes is stronger for an incident-light polarisation parallel to the [001] direction (Fig. 2d). The $\Theta_{\mathrm{spectro}}$ angle ranges between 25 and 50°, with some configurations exhibiting a more significant canting with respect to the [001] direction. Due to the low symmetry of the local environment of the OH group (Fig. 1) and related anisotropy of the Born effective charge tensor, the $\Theta_{\mathrm{spectro}}$ angle can differ from the $\Theta_{\mathrm{stretch}}$ angle. For most of the models, the difference is small, not exceeding 10°(Fig. 2d). The Fe_3 configuration is anomalous, with a $\Theta_{\mathrm{spectro}}$ angle of 86°, corresponding to a polarisation almost perpendicular to the [001] direction, and a $\Theta_{\mathrm{stretch}}$ angle indicating a canting of only 54°. This discrepancy can be traced back to a relatively large off-diagonal $Z^*_{\mathrm{H},zy}$ element (0.45 electron charge) which counterbalances the contribution of the diagonal $Z^*_{\mathrm{H},zz}$ (0.74 electron charge) element to the polarisation change induced by the longitudinal displacement of the hydrogen. As the Born effective charges are dynamical charges accounting for the changes in

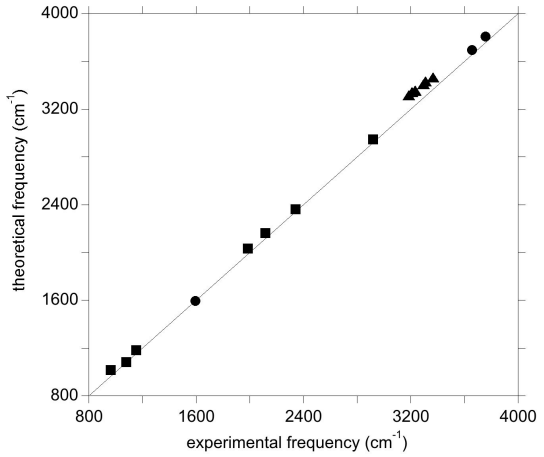

Figure 3. Theoretical vs. experimental vibrational frequencies of water (circles), diaspore (squares), and OH-bearing Al vacancies associated with Ti in corundum from Balan (2020) (triangles).

the electronic structure related to atomic displacements (e.g. Ghosez et al., 1998), the anomalous behaviour observed in the Fe_3 configuration suggests a significant electronic interaction between the nearby Fe^{2+} cation and the hydrogen atom.

3.2 Discrepancies between theoretical and experimental frequencies: calculated properties of benchmark systems

Theoretical and experimental frequencies are not expected to match perfectly due to the many approximations used in the theoretical modelling. These discrepancies can be assessed using two "benchmark" systems – water and diaspore (AlOOH), which suggest that the theoretical frequencies are affected in a systematic manner (Fig. 3).

For the isolated water molecule, the theoretical harmonic OH stretching frequencies are a few dozens of wavenumbers higher than their experimental counterparts (Table S1 in the Supplement). This confirms the approximate cancellation of errors arising from the use of the PBE exchange–correlation functional and the neglect of anharmonicity (Balan et al., 2007). Compared with the stretching modes, the theoretical frequency of the H_2O bending mode is closer to its experimental counterpart (Table S1). Calculations performed on diaspore (AlOOH), which displays medium-strength hydrogen bonds, lead to an OH stretching frequency at $\sim 2920\,cm^{-1}$ and OH bending frequencies between 960 and $1153\,cm^{-1}$ (Table S2). The experimental OH stretching band is significantly broadened ($> 200\,cm^{-1}$) by anharmonic interactions even in highly ordered samples, whilst the bending bands are less affected (Delattre et al., 2012). A rough comparison indicates that the theoretical frequencies overestimate those of experimental bands by less than $60\,cm^{-1}$. The diaspore spectrum also displays several bands between 1980 and $2340\,cm^{-1}$ whose frequencies are about twice that of the fundamental bending bands and which have been interpreted as two-phonon excitations involving the OH bending modes (Stegmann et al., 1973; Kohler et al., 1997; Delattre et al., 2012). Although not fully explained, their anomalous intensity is likely related to a stronger anharmonic character stemming from the significant hydrogen bonding in diaspore (Kohler et al., 1997). Notably, the experimental frequencies of these bands are within $50\,cm^{-1}$ of those obtained by multiplying the fundamental theoretical frequency of the IR-active OH bending modes by 2 (Table S2, Fig. 3). Previous investigations of OH defects into corundum (Fig. 3) and quartz have shown similar agreement between theoretical and experimental frequencies, where theoretical OH stretching frequencies were found to overestimate their experimental counterparts by ~ 10 to $\sim 130\,cm^{-1}$ (e.g. Jollands et al., 2020; Balan, 2020).

Table 3. Theoretical and experimental OD stretching frequencies. Experimental frequencies were assessed from Müller and Günthard (1966) for Co and Ni and from Ramírez et al. (1997) for the Mg-doped sample.

Model	ω_{OD} theoretical (cm^{-1})	ω_{OD} experimental (cm^{-1})
Mg_1	2181	2228
Mg_2	2215	–
Mg_3	2340	–
Mg_4	2325	2228
Co_1	2212	2246
Co_2	2195	–
Co_3	2305	2288
Co_4	2339	2318
Ni_1	2185	2221
Ni_2	2218	–
Ni_3	2355	2305
Ni_4	2285	2221

3.3 Assignment of vibrational bands associated with divalent cations

The room temperature spectra of synthetic sapphire containing Mg^{2+}, Ni^{2+} and Co^{2+} ions, along with hydrogen, display a broad band at $\sim 3000\,cm^{-1}$ and a series of well-defined bands at lower frequency (Müller and Günthard, 1966; Volynets et al., 1972; Ramírez et al., 1997; Fukatsu et al., 2003).

When attempting to assign such bands to a given defect, it is important to note that, in cases of significant hydrogen bonding, the OH stretching bands are frequently affected by interactions with lower-frequency modes. This leads to their broadening and modification of their shapes (e.g. Nibbering et al., 2007). For this reason, it is not straightforward to as-

sign the OH stretching bands to specific configurations of OH groups. In comparison, the narrower OD bands can be more easily related to specific models (Table 3), which then helps to guide assignment of OH bands.

Another challenge is that the composition of synthetic samples is not fully documented. This is problematic as hydrous defects can be associated with chemical impurities at very low concentration levels. For example, the Verneuil samples investigated by Beran (1991) and the Fe-doped sample of Eigenmann and Günthard (1971) display the "3309 cm^{-1} series" of bands related to the occurrence of OH groups associated with Al vacancies and charge-compensating Ti^{4+} cations (Moon and Phillips, 1991, 1994; Balan 2020). This may explain why the spectrum of the Fe-doped sample investigated by Eigenmann and Günthard (1971) significantly differs from that of the Co- and Ni-doped samples, whilst those of the Fe-doped, Fe : Ti-doped and Ti-doped samples are similar.

However, despite these issues, attempts are made to assign the experimentally observed bands to specific defect configurations, using evidence from both DFT modelling and analyses of correlations in band areas between multiple experimental spectra.

3.3.1 Cobalt

The room temperature spectrum of Co-doped synthetic sapphire (Fig. 4a) displays a broad band at $\sim 3029\,cm^{-1}$, as well as narrower and weaker bands at 2530, 2425, 2375 and 1990 cm^{-1} (Müller and Günthard, 1966). Here and in the following, wavenumbers have been determined from digitised spectra; therefore peak positions may be inaccurate. At 77 K, the band at 3029 cm^{-1} splits into three narrower components at 3061, 3014 and 2955 cm^{-1} and a narrower band is observed at 2717 cm^{-1}. An additional broad band at 3225 cm^{-1} in the 77 K spectrum is likely related to ice in the low-temperature cell (Fig. 4a). The OD bands are observed at ~ 2318, ~ 2288 and $\sim 2246\,cm^{-1}$. Assuming that the ratio of the OH to OD frequencies is 1.35, which is based on the value reported for an Mg-doped sample by Ramírez et al. (1997), these bands would correspond to OH stretching frequencies at 3129, 3089 and 3032 cm^{-1}, respectively. Based on their relative frequencies, the three OD bands can be ascribed to the Co_4, Co_3 and Co_1 configurations, respectively (Table 3, Fig. 4b). The corresponding bands are not resolved in the broad OH stretching band centred at 3029 cm^{-1}, although the band appears to be asymmetric, suggesting that it may be composed of multiple individual bands, with a major component at 3029 cm^{-1}. The 3029 cm^{-1} experimental frequency is close to that theoretically inferred for the Co_1 configuration. This suggests that this configuration is dominant, which is consistent with the relative stability of the Co-bearing configurations (Table 1). Regarding the lower-frequency bands, the experimental 2425 and 2375 cm^{-1} bands approximately match the theoretical harmonic frequencies of the first overtone of the δ bending modes of the more stable Co_1 and Co_4 configurations (Table 1), whilst the experimental 1990 cm^{-1} band (Fig. 4a) could be related to the overtone of the δ bending mode of the Co_3 configuration (Fig. 4b). This interpretation is consistent with the occurrence of the three configurations inferred from the analysis of the OD bands. Using the same interpretative framework, the 2955, 2717 and 2533 cm^{-1} bands, present in the Müller and Günthard (1966) 77 K spectrum (Fig. 4a), could correspond to the second overtones of the Co_1 δ, Co_3 γ and Co_4 γ bending modes, respectively, enhanced by their interaction with the fundamental OH stretching excitation.

3.3.2 Nickel

The main band at $\sim 3000\,cm^{-1}$ is split in the room temperature spectrum of Ni-doped corundum (Fig. 5a), with two maxima experimentally observed at ~ 3015 and $\sim 2970\,cm^{-1}$ (Müller and Günthard, 1966). This doublet is also observed in the 14 spectra from high-Ni synthetic sapphires recorded at the GIA (Fig. 5b), which show maxima positions from 3012 to 3016 cm^{-1} and from 2966 to 2972, respectively. Additional contributions are resolved at 2927 and 2851 cm^{-1} at 77 K.

Two OD bands (Fig. 5a) are observed at ~ 2305 and $\sim 2221\,cm^{-1}$, which would correspond to OH stretching frequencies of 3112 and 2998 cm^{-1}, respectively. The 2998 cm^{-1} frequency falls between the two experimental bands at ~ 2970 and $\sim 3015\,cm^{-1}$. Comparing experimental and theoretical frequencies (Table 1), these two OH stretching bands can be ascribed to the Ni_1 configuration and the slightly less stable Ni_4 configuration, respectively, whilst the corresponding OD bands are not resolved in the experimental peak at 2221 cm^{-1} (Table 3). The peak inferred from the OD band at 3112 cm^{-1} is not resolved in the OH stretching spectrum but could contribute to the high-frequency tail of the broad OH stretching band. Considering its higher frequency, an inferred 3112 cm^{-1} band would correspond to the Ni_3 configuration (Fig. 5d).

Considering the lower-frequency region, Müller and Günthard (1966) presented a spectrum showing bands at 2444, 2388, 2259 and 2006 cm^{-1} (Fig. 5a). The 14 spectra from the GIA database show bands at 2010, 2131, 2260, 2392, 2402 (weak), 2450, 2471 and 2743 cm^{-1} (the frequencies are those determined from the spectrum reported in Fig. 5b). As the positions of the Müller and Günthard (1966) bands were extracted from a spectrum digitised from a scanned document, it is likely that their 2444, 2388, 2259 and 2006 cm^{-1} bands correspond to the bands at 2450, 2392, 2260 and 2010 cm^{-1} in the GIA spectrum (Fig. 5b). The latter positions are assumed to be correct herein. From the 14 GIA spectra, Pearson's correlation coefficients (p) between the area of the main band comprising the ~ 2970 and $\sim 3015\,cm^{-1}$ doublet and the low-frequency bands are

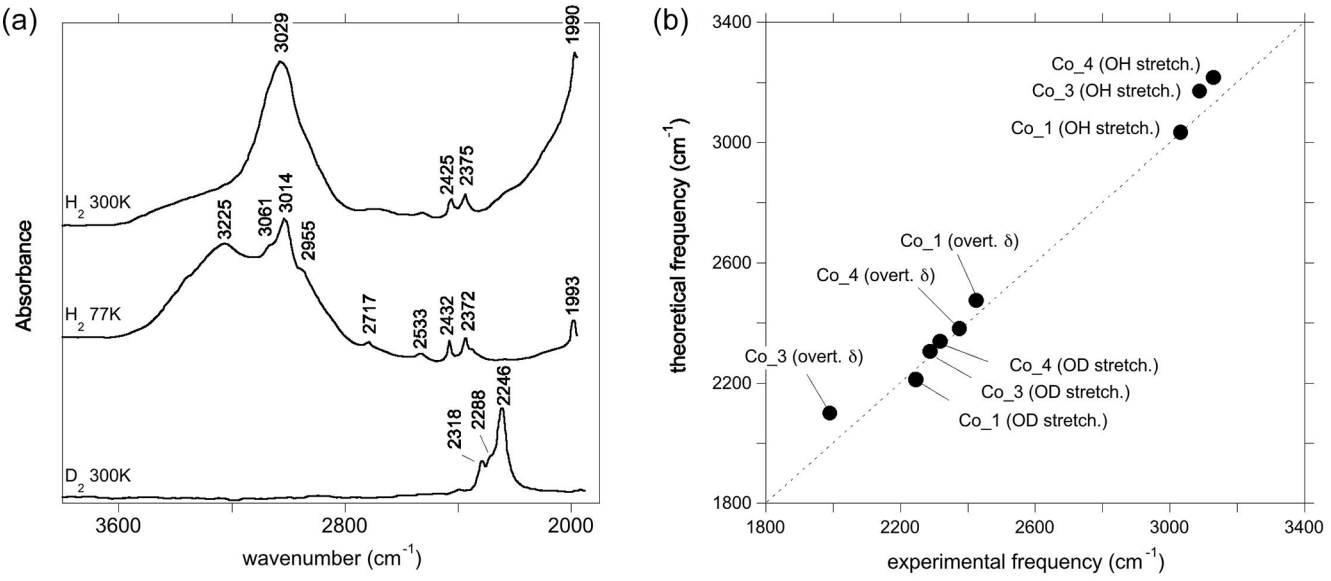

Figure 4. (a) Experimental spectra of Co^{2+}-bearing corundum from Müller and Günthard (1966). H_2 and D_2 refer to the gases in which Co^{3+} was reduced. The values 300 and 77 K refer to the temperature at which the spectra were recorded. These spectra were digitised from the original publication, so band positions may be inaccurate. **(b)** Comparison of theoretical with experimental frequencies. The experimental Co_4 and Co_3 stretching frequencies have been inferred from the position of OD bands. OH stretch: OH stretching frequency; OD stretch: OD stretching frequency; overt. δ: first overtone of δ bending modes (Table 1).

as follows: $2010\,cm^{-1}$, $p = 0.97$; $2131\,cm^{-1}$, $p = 0.71$; $2260\,cm^{-1}$, $p = 0.96$; $2392\,cm^{-1}$, $p = 0.79$; $2402\,cm^{-1}$, $p = 0.59$; $2450\,cm^{-1}$, $p = 0.93$; $2471\,cm^{-1}$, $p = 0.86$; and $2743\,cm^{-1}$, $p = 0.96$. The strong correlations between the main band and the 2010, 2260 and $2450\,cm^{-1}$ bands are consistent with these bands being present in the Müller and Günthard (1966) 300 K spectrum, although the $2392\,cm^{-1}$ band, observed in the latter, shows a relatively weak correlation (Fig. 5c). It is possible that the poorer correlation is due to the proximity of this band to the signal associated with atmospheric CO_2 in routine FTIR measurements, which complicates baseline subtraction.

The two narrow bands at 2450 and $2010\,cm^{-1}$, which are both present in the Müller and Günthard (1966) spectrum (Fig. 5a) and show strong correlations with the main band in the spectra from the GIA database, can be assigned to the first overtone of the δ bending modes of the Ni_1- and Ni_3-bearing models, respectively (Fig. 5d). The theoretical position of the first overtone of Ni_4 is $2423\,cm^{-1}$, which would be consistent with the $2392\,cm^{-1}$ experimental band, although the correlation is less strong than for the 2450 and $2010\,cm^{-1}$ bands.

The assignment of the 2260, 2471 or $2743\,cm^{-1}$ experimental bands is not straightforward. Their strong correlations suggest that they are related to defects associating Ni and H atoms and rule out a potential assignment to another impurity. In addition, their systematic occurrence and limited number suggest that they are related to some of the four neutral configurations investigated (Table 1) as the location of the H atom on other oxygen anions would lead to significant overbonding. Therefore, and as for the Co-doped samples, these bands most likely correspond to higher-order overtones of vibrational modes involving the hydrogen atom. In particular, the experimental $2260\,cm^{-1}$ band is consistent with the frequency of the second overtone of the theoretical mode at $756\,cm^{-1}$ (second overtone at $2268\,cm^{-1}$), which occurs in both the Ni_3 and the Ni_4 configurations and displays an unexpectedly large hydrogen contribution in its atomic displacement vectors (Table 2). The properties of such a specific mode depend on the respective properties of the crystal host and molecular impurity. Although no clear explanation for its absence in the spectrum of the Co-doped sample of Müller and Günthard (1966) can be proposed, it is not unlikely that the difference between the Ni and Co spectra is related to small variations in vibrational properties that are not perfectly reproduced in the theoretical models.

3.3.3 Magnesium

Similar to, but offset from, the Ni-doped sample, a broad band centred at $\sim 3000\,cm^{-1}$, with maxima at 3027 and $2991\,cm^{-1}$, is observed in the infrared spectrum of the Mg-doped sample investigated by Fukatsu et al. (2003) with an additional weaker band at $3232\,cm^{-1}$ (Fig. 6a). The main band is stronger when the electric field is parallel to the [001] direction (Volynets et al., 1972; Fukatsu et al., 2003). An OD band at $\sim 2228\,cm^{-1}$ with a width of $56\,cm^{-1}$ was reported by Ramírez et al. (1997). Its frequency and width are con-

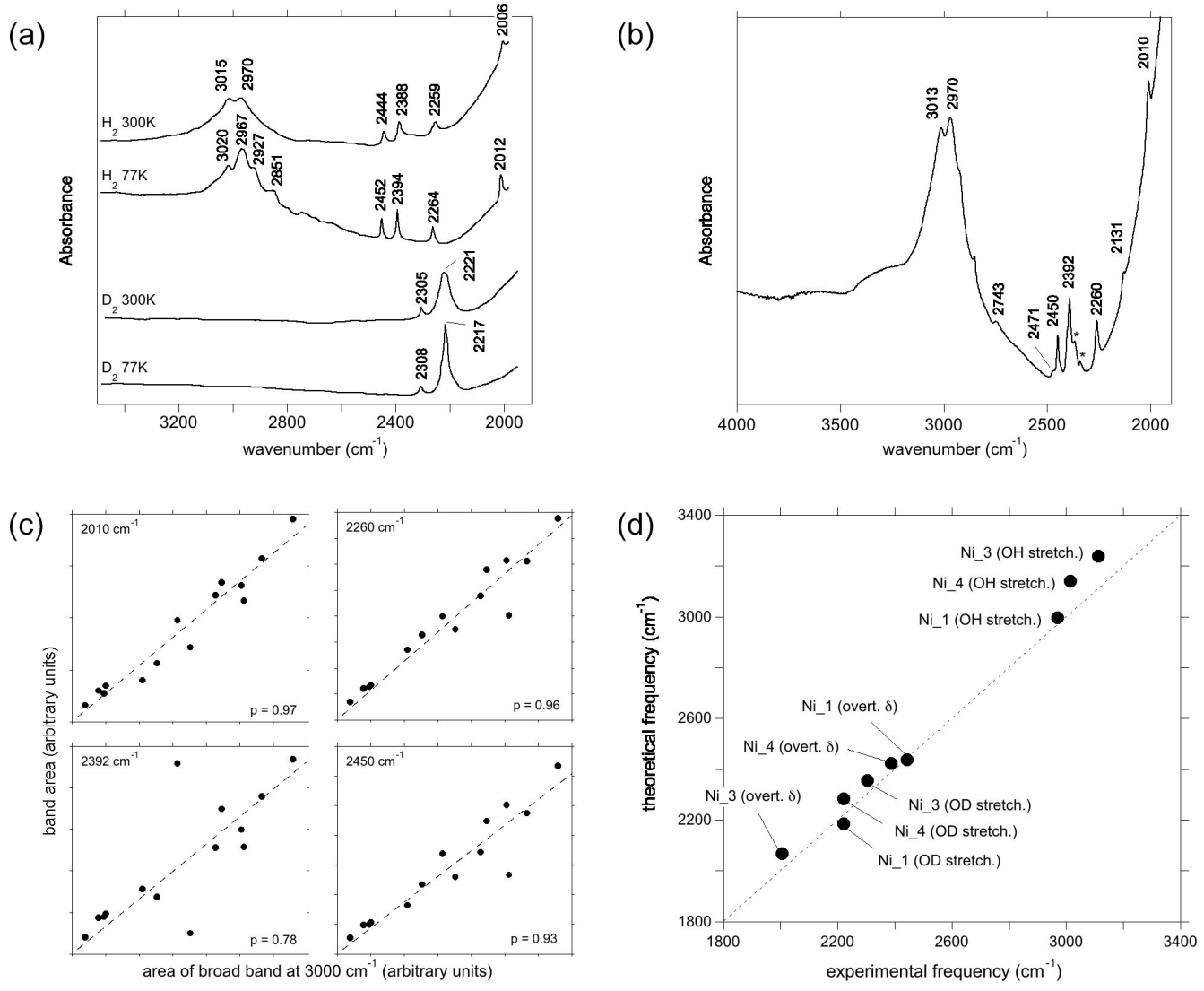

Figure 5. **(a)** Experimental spectra of Ni^{2+}-bearing corundum, synthesised by Ni^{3+} reduction, from Müller and Günthard (1966). H_2 and D_2 refer to the gases in which Ni^{3+} was reduced. The values 300 and 77 K refer to the temperature at which the spectra were recorded. These spectra were digitised from the original publication, so band positions may be inaccurate. **(b)** Spectrum of a synthetic Ni-bearing sample from the GIA database. The asterisks denote artefactual bands related to atmospheric CO_2. The positions in this spectrum are taken as the correct positions; e.g. 3015 cm^{-1} in **(a)** is equivalent to 3013 cm^{-1} in **(b)**. **(c)** Selected correlations of the areas of some low-frequency bands with the area of the broad OH stretching band centred at $\sim 3000\,cm^{-1}$, along with their Pearson's correlation coefficient (p) values and linear regressions. **(d)** Comparison of theoretical with experimental frequencies. Labels as in Fig. 4b. The experimental Ni_3 stretching frequency has been inferred from the position of the OD band.

sistent with the two OH stretching bands experimentally observed at 3027 and 2991 cm^{-1} by Fukatsu et al. (2003). Following the assignments proposed for the Ni- and Co-doped samples, these two OH stretching bands can be assigned to the two most stable configurations, Mg_4 and Mg_1 (Table 1).

The lower-frequency bands in the hydrogenated Mg-doped sample are reported at 2030, 2140, 2254, 2416 and 2462 cm^{-1}, and a broader one is reported at 2628 cm^{-1} (Fukatsu et al., 2003). The GIA spectra show the same bands, as well as small bands at 2482 and 2567 cm^{-1}, the former being a shoulder on the stronger 2462 cm^{-1} band (Fig. 6a). The experimental bands at 2028, 2254, 2416 and 2628 cm^{-1} are well correlated to the main band at $\sim 3000\,cm^{-1}$ (Fig. 6b).

Considering that the Mg_1 model has the greatest stability and based on its frequency, the experimental band at 2628 cm^{-1} is ascribed to the δ OH bending overtone of the Mg_1 configuration (Table 1, Fig. 6c). Its broadening suggests a more significant coupling of the fundamental OH stretching transitions with the bending overtones when

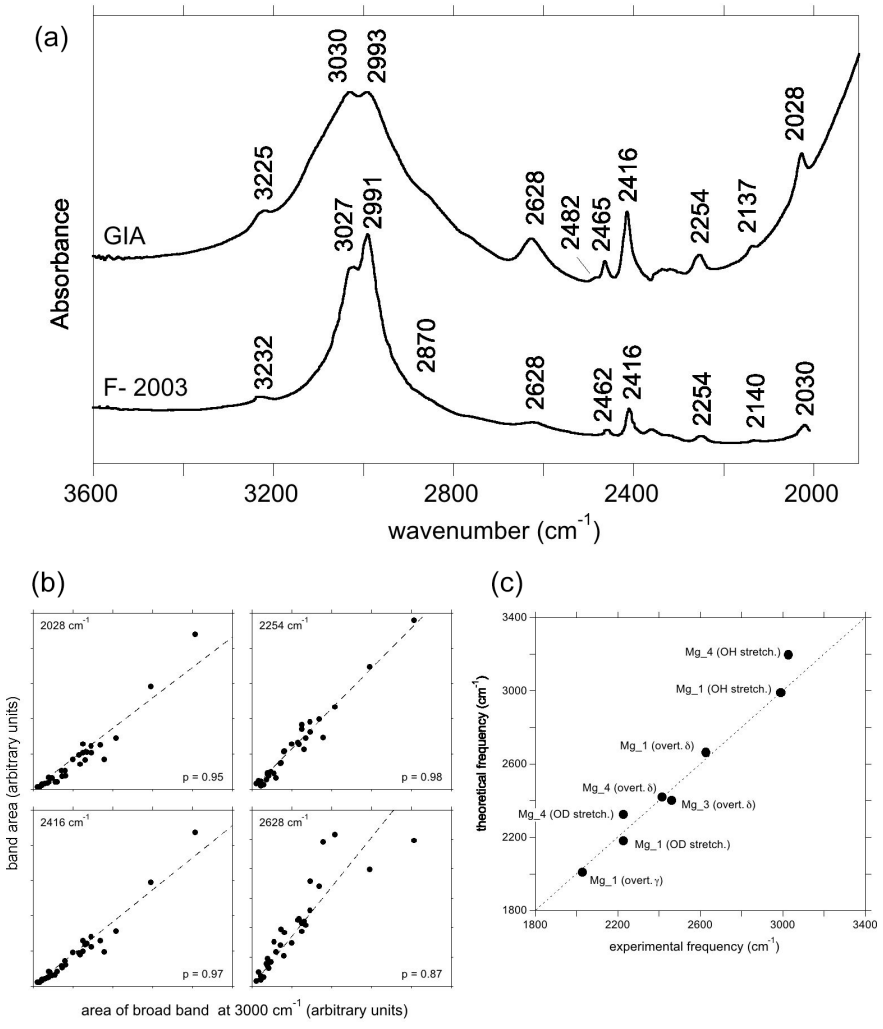

Figure 6. (a) Experimental spectra of Mg^{2+}-bearing corundum from Fukatsu et al. (2003) (bottom) and from the GIA database (top). The lower spectrum was digitised, so positions may be inaccurate. The positions in the top spectrum are taken to be correct; e.g. 2137 and 2993 $^{-1}$ in the top spectrum are equivalent to 2140 and 2991 cm^{-1} in the lower spectrum. **(b)** Selected correlations of the area of the low-frequency bands with that of the broad OH stretching band centred at $\sim 3000\,cm^{-1}$, as in Fig. 5c. **(c)** Comparison of theoretical with experimental frequencies. Labels as in Fig. 4b, with the addition of overt. γ (first overtone of the γ bending mode).

both frequencies begin to overlap. The experimental band at $2028\,cm^{-1}$ matches the overtone of the γ OH bending mode of the Mg_1 configuration (Table 1), whilst the $2416\,cm^{-1}$ band would correspond to the overtone of the δ OH bending mode of the Mg_4 configuration. As with the Ni-doped corundum, the band at $2254\,cm^{-1}$ is likely related to the second overtone of the coupled mode with significant hydrogen contribution calculated at $755\,cm^{-1}$ for the Mg_4 configuration (Table 2).

3.3.4 Beryllium: a reappraisal

Experimental spectra of sapphires treated by Be diffusion sometimes display a broad band at $\sim 3060\,cm^{-1}$ with a dominant polarisation parallel to the [001] direction. This band is usually associated with a band at $2490\,cm^{-1}$, which has similar pleochroism and is most likely also related to a Be-bearing defect (Fig. 7a). Theoretical modelling of Be incorporation in corundum provided strong support for the assignment of the $3060\,cm^{-1}$ band to the OH stretching mode of an electrostatically neutral defect in which the Be occupies the basal plane of an Al vacant site and an OH group, related to the coupled incorporation of hydrogen, forming a H bond along the edge of the vacant site ($(Be)_{Al}$–OH_{in}) (Jollands and Balan, 2022). The formation of short Be–O bonds and location of the Be atom on the basal plane of the Al site, which is also consistent with the theoretical findings of Futazuka et al. (2020), lead to a different local configuration of the hydrous defect compared to that observed for the incorporation of the other divalent cations. The various configurations of this defect have been theoretically investigated

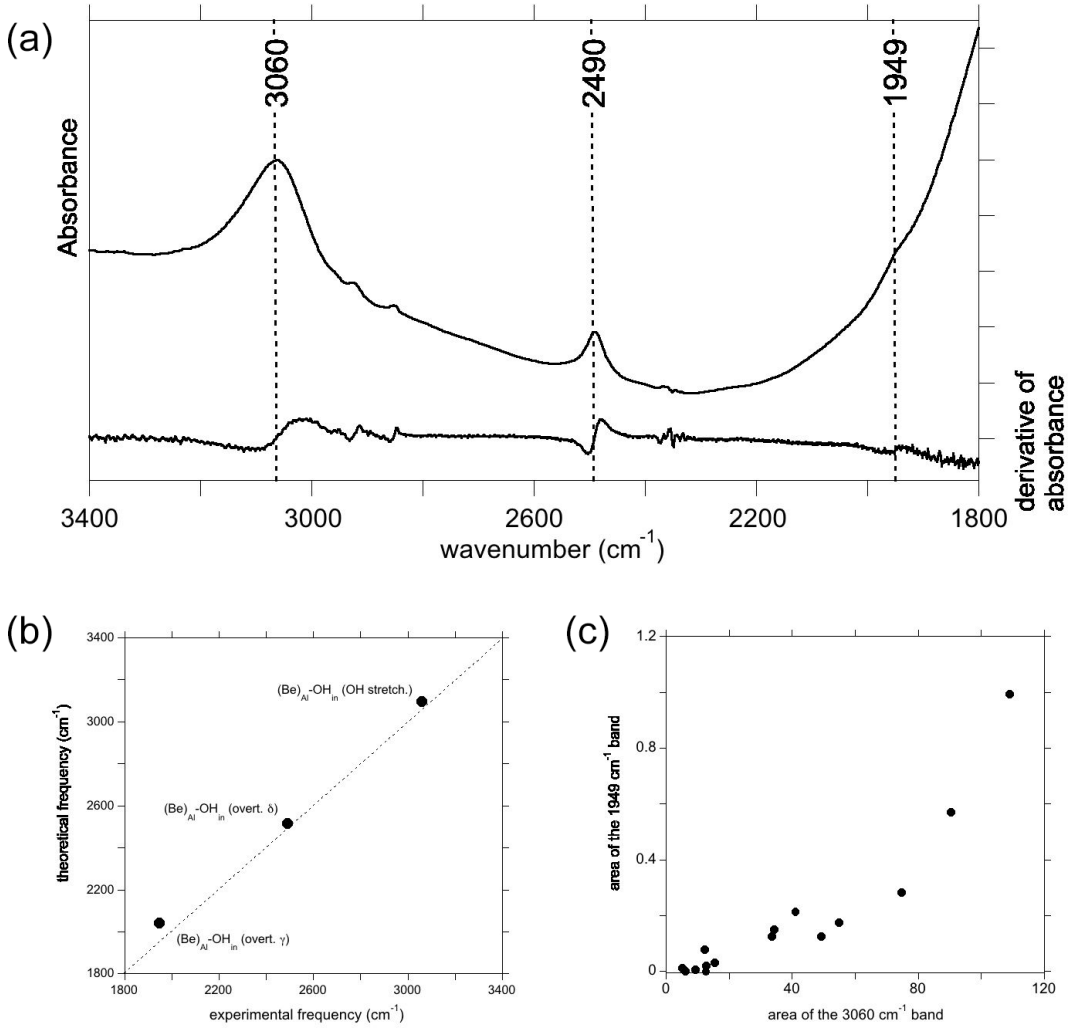

Figure 7. (a) Spectrum recorded from a Be^{2+}-bearing corundum from the GIA database, along with the first derivative of the spectrum, used for identifying the presence of a band at 1949 cm^{-1}. **(b)** Comparison of theoretical with experimental frequencies, labels as in Figs. 4b and 6c. **(c)** Correlation of the area of the band at 1949 cm^{-1} with that of the OH stretching band at 3060 cm^{-1}.

in Jollands and Balan (2022), and only the most stable one is considered here. Based on a comparison with other X–H vibrational frequencies and on the theoretical properties of a Be–H model, the band at 2490 cm^{-1} was ascribed to the formation of Be–H groups (Jollands and Balan, 2022). Although the high-temperature Be treatment of corundum may be done in reduced conditions, which would also lead to the formation of Ti^{3+} ions in Fe–Ti sapphire (Rossi et al., 2022), the systematic presence of this band in samples presumably treated under different conditions was unclear. Considering the presence of absorption bands in the same frequency range as that associated with other divalent cations that are unlikely to form strong X–H bonds, the present theoretical results support the alternative assignment of the 2490 cm^{-1} band to a bending overtone of the $(Be)_{Al}$–OH_{in} configuration. This has a theoretical harmonic frequency of 2514 cm^{-1}, very close to its experimental counterpart (Fig. 7b). Simply, contrary to the findings of Jollands and Balan (2022), Be–H bonds are not necessary to explain the 2490 cm^{-1} band. In this case, the lack of perfect correlation between the intensities of the main OH stretching band and 2490 cm^{-1} band could be related to the presence of other divalent cations in the samples belonging to the large database investigated by Jollands and Balan (2022), forming defects contributing to the broad band at 3000 cm^{-1}. Finally, the overtone of the other bending mode (γ) of the $(Be)_{Al}$–OH_{in} model is predicted to occur at 2040 cm^{-1} (Table 1). A careful examination of the experimental spectra of Be-diffused samples revealed a weak feature at 1949 cm^{-1}, which is broadly correlated to the main band at 3060 cm^{-1} (Fig. 7c) and occurs in an admissible frequency range (Fig. 7b). It is therefore most likely that this weak band, easily missed and previously not reported, correspond to the other bending overtone of the $(Be)_{Al}$–OH_{in} configuration. Its presence confirms the theoretical predic-

tion and further supports the assignment of the FTIR spectroscopic features observed between 1900 and 2700 cm^{-1} in corundum to overtones of OH bending modes.

3.3.5 The "3161 cm^{-1}" band

The infrared spectrum of the natural yellow sapphire (YS-1) sample (Fig. 8a) is similar to those reported by, for example, Smith and Van der Bogert (2006) and Choudhary and Vijay (2018). It displays three well-defined bands at 3163 cm^{-1} (herein referred to as the 3161 cm^{-1} band for consistency with the literature), 3242 and 3355 cm^{-1}, with the former superimposed on a broader shoulder centred at around 3070–3100 cm^{-1}. A small band at 3302 cm^{-1} is also present in the spectra from the GIA database. This type of spectrum may be encountered in Fe-rich and Ti-poor natural sapphires and some rubies. In terms of crystals analysed at laboratories of the GIA, the most common main hue for corundum containing this band is yellow, with red, pink, orange and blue hues comprising the remainder (Fig. 8a). The main bands have a stronger intensity when the incident-light polarisation is perpendicular to the (001) plane (Fig. 8a). This suggests that the related OH groups are not associated with the basal plane of Al vacancies (Balan, 2020) but that they more likely correspond to interstitial H^+ compensating for the electrostatic charge imbalance caused by substitution of divalent or monovalent cations for trivalent aluminium. A low-frequency band is consistently observed at 2420 cm^{-1}. Analysis of correlations from 250 spectra from the GIA database shows a very strong positive correlation between the areas of the 3161 and 2420 cm^{-1} bands ($p = 0.99$). Two other low-frequency bands are consistently observed at 2459 and 2480 cm^{-1}, albeit with poorer correlations with the 3161 cm^{-1} band ($p =$ 0.93 and 0.77, respectively). The area of the 2459 cm^{-1} band shows the strongest correlations with the $\sim$ 3100 ($p = 0.95$), 3242 ($p = 0.96$) and 3355 cm^{-1} ($p = 0.95$) bands.

The correlation between the areas of the 3161 and 2420 cm^{-1} bands suggests that they are related to the same OH configuration (Fig. 8b). As the samples displaying the "3161 series" can be iron-rich and titanium-poor (e.g. Schwarz et al., 2008), it may be reasonable to assign the main bands to OH groups in association with Fe^{2+} ions. Among the potential configurations, the Fe_4 configuration has theoretical OH stretching and bending overtone frequencies of 3231 and 2352 cm^{-1}, respectively, which are in the admissible range with respect to the experimental 3161 and 2420 cm^{-1} frequencies (Fig. 8c). The Fe_1 configuration, which is moderately more stable (by 3 kJ mol^{-1}) than the Fe_4 configuration, could then lead to an OH stretching band contributing to the broad signal at $\sim$ 3100 cm^{-1} and to the OH bending overtone at 2459 cm^{-1} (Fig. 8a).

The experimental bands at 3242, 3355 and 3302 cm^{-1} cannot be assigned to specific defects, although all are correlated with the 3161 cm^{-1} band ($p = 0.96$, 0.90 and 0.85, respectively). The relatively poor correlation between 3161 and 3302 cm^{-1} bands is likely due to the very low absorbance of the latter, as well as its location on the shoulder of the 3161 cm^{-1} band. Together, these observations suggest that these bands are related to similar defects, meaning defects with the same stoichiometry ($Fe^{2+}OH$). They could result from the anharmonic interaction of the OH stretching mode with higher-order overtones (Fermi resonances) or with low-frequency excitations (combination bands).

The area of the experimental band at 2480 cm^{-1} does not correlate well with any other bands, suggesting that it might not be genetically related to the 3161 cm^{-1} band, i.e. does not have $Fe^{2+}OH$ stoichiometry, despite generally being present in the spectra containing the "3161 cm^{-1} series".

Significant spectral changes are reported in heating experiments of samples corresponding to the "3161 cm^{-1} series": a sample heated in oxidising atmosphere at 900 °C for 6 h displays a spectrum of the Punsiri type, whilst a flat spectrum is observed on same sample heated at 1550 °C for 6 h (Atikarnsakul and Emmett, 2021). Based on the assignment of the "3161 cm^{-1} series" to an Fe^{2+}–OH defect, these changes could be interpreted as follows. Heating at 900 °C at ambient pressure leads to oxidation of Fe^{2+} to Fe^{3+} ions, which mobilises the H^+ that is associated with Fe^{2+}. Some H^+ may diffuse out of the crystal, and some could combine with Mg^{2+} ions at trace concentration level. This forms an Mg^{2+}–OH defect, leading to a Punsiri-type spectrum similar to that observed in Mg-doped samples. Further heating of the sample at 1550 °C then leads to full dehydration, associated with formation of the associated Mg^{2+}–hole pairs, explaining the enhancement of the yellow colour.

3.4 Qualitative properties of OH bending overtones in H-bonded systems

The assignment of the low-frequency bands to overtones of bending modes requires further explanations for two observations: (i) the intensity of the low-frequency bands is anomalously high for overtone bands compared with that of the fundamental OH stretching bands observed in the same spectra; (ii) the polarisation of the overtone bands is similar to that of the fundamental stretching bands (Fukatsu et al., 2003; Jollands and Balan, 2022). Assuming that the proposed assignments are correct, both peculiarities are likely related to the significant H bonding of the interstitial H atoms. Although infrequent, strong two-phonon bands related to the bending modes have been observed in diaspore (AlOOH) and groutite (MnOOH), which are hydrous minerals with medium-strength H bonds (Stegmann et al., 1973; Kohler et al., 1997; Delattre et al., 2012). Abnormally strong bending overtones have also been reported in H-bonded molecular systems, such as chloroform ($CHCl_3$) and cesium bihalide salts (Thompson and Pimentel, 1960; Nibler and Pimentel, 1967). Even though they did not propose an interpretation for the low-frequency bands, it is noteworthy that Müller and

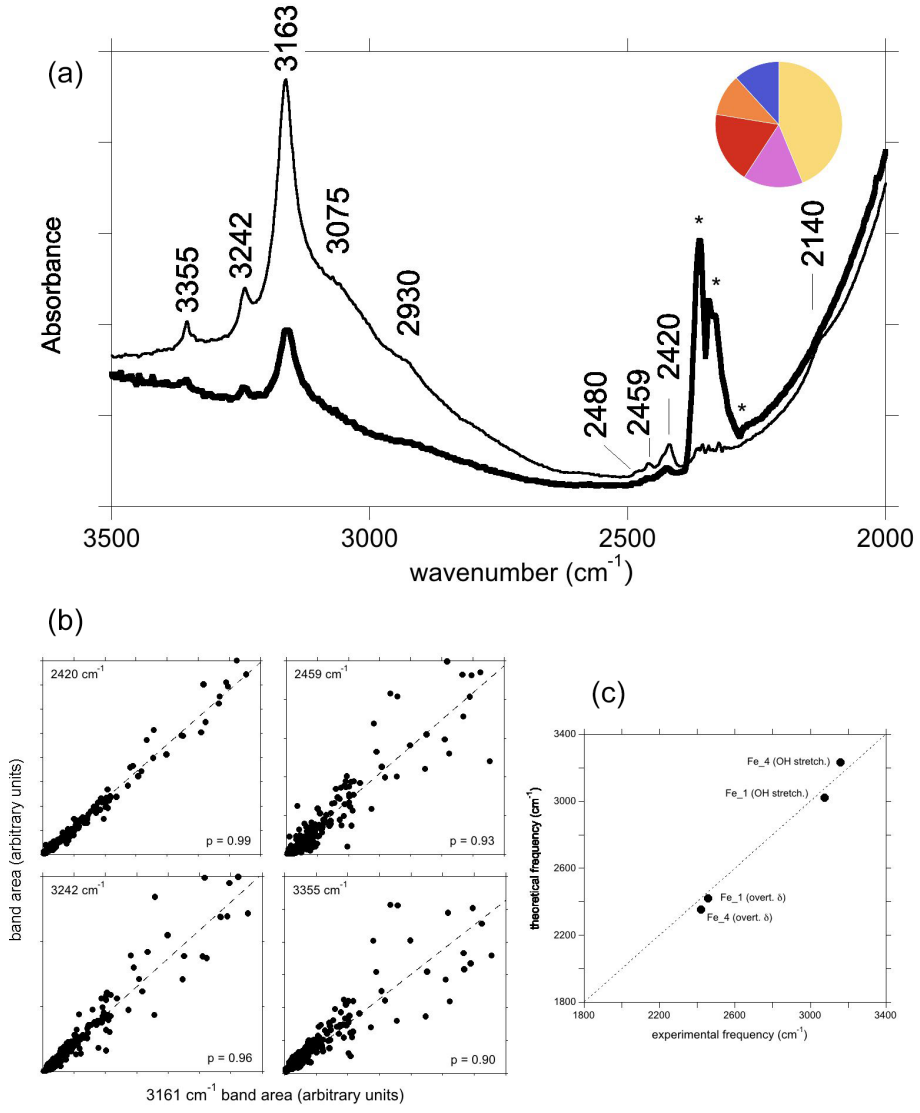

Figure 8. (a) Spectrum of natural yellow sapphire (YS-1) from Sri Lanka for a beam polarisation approximatively parallel (thin line) or perpendicular (thick line) to the [001] direction. The asterisks denote artefactual bands related to atmospheric CO_2. The inset is a simple colour pie chart showing the distribution of hues, describing crystals with the "3161 cm^{-1}" band from the GIA database ($\sim$ 15 000 samples). A majority are in the yellow–orange–red–pink range, and only a minority are blue. **(b)** Correlations of the area of selected bands with that of the 3161 cm^{-1} band. **(c)** Comparison of theoretical with experimental frequencies assuming that the observed bands are related to Fe^{2+} cations.

Günthard (1966) stated that the OH···O environment in reduced sapphire is analogous to the bihalide system $(FHF)^-$.

Following Thompson and Pimentel (1960) and Nibler and Pimentel (1967), an anomalous intensity of the OH bending overtone can be qualitatively discussed using a local molecular picture. This is consistent with the isolated character of the hydroxylated defects investigated in this present study. The transition intensity depends on the specific expression of the dipole moment function, as well as on the shape of the potential, which determines the vibrational wave functions (e.g. Thompson and Pimentel, 1960). Assuming that only the ground state is significantly populated at room temperature, the transition from the $n = 0$ to $n = 1$ state corresponds to a fundamental transition, whilst overtones correspond to transitions from $n = 0$ to $n > 1$ states. Only transitions with $\Delta n = \pm 1$ are allowed in the harmonic approximation, whereas overtones can arise from the nonlinearity of the dipole moment function (electrical anharmonicity) and from the anharmonicity of the potential (mechanical anharmonicity). Although a full treatment of the overtone absorption intensities is beyond the objectives of the present study, a conceptual understanding of the H-bonded system can be obtained using a simple molecular model with two vibrational degrees of freedom (Thompson and Pimentel, 1960).

Table 4. Proposed assignments of infrared absorption bands in the spectra of corundum containing divalent cations. ME: multiple excitation (anharmonic resonance or combination band involving the strong OH stretching excitation); HOCM: higher-order overtone of coupled mode (see text). δ and γ correspond to the first overtone of corresponding bending modes; ? corresponds to an undefined interpretation.

Sample	Experimental frequency (cm^{-1})	Theoretical frequency (cm^{-1})	Interpretation	Experimental frequency (cm^{-1})	Theoretical frequency (cm^{-1})	Interpretation
Ni-doped	3013	3140	Ni_4	2450	2438	Ni_1 (δ)
	2970	2997	Ni_1	2392	2423	Ni_4 (δ)
				2260	2268	HOCM
				2010	1939	Ni_3 (δ)
Co-doped	3029	3034	Co_1	2530	–	?
				2425	2475	Co_1 (δ)
				2375	2381	Co_4 (δ)
				1990	1917	Co_3 (δ)
Mg-doped	3225	–	?	2628	2663	Mg_1 (δ)
	3030	3196	Mg_4	2465	2401	Mg_3 (δ)
	2993	2990	Mg_1	2416	2419	Mg_4 (δ)
				2254	2265	HOCM
				2137	–	?
				2028	2010	Mg_1 (γ)
"3161 series"	3355	–	ME ?	2480	–	?
	3242	–	ME ?	2459	2420	Fe_1 (δ)
	3163	3231	Fe_4	2420	2352	Fe_4 (δ)
	3075	3020	Fe_1			
Be-diffused	3060	3096	$(Be)_{Al}$–OH_{in}	2490	2514	$(Be)_{Al}$–OH_{in}(δ)
				1949	2040	$(Be)_{Al}$–OH_{in}(γ)

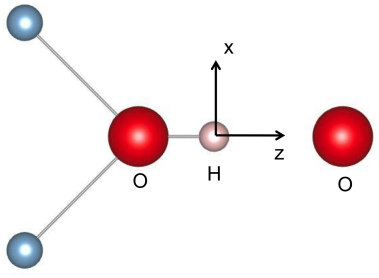

Figure 9. Simple molecular model with C_{2v} symmetry of a H-bonded OH group. A qualitative discussion of the OH vibrational properties can be restricted to the displacement of the H atom in the z (longitudinal) and x (transverse) directions, corresponding to the stretching and bending vibrations, respectively.

This model with C_{2v} (mm2) symmetry displays an OH group oriented along the z axis sharing a H bond with a facing O atom (Fig. 9). The OH stretching mode mostly corresponds to a small longitudinal displacement (dz) of the H atom from its equilibrium position along the z direction, whilst the in-plane bending mode corresponds to its transverse displacement (dx). In such a model, the intensity and polarisation properties of the first bending overtone are determined by the longitudinal component of the dipole moment function, whilst the fundamental bending transition depends on the transverse component (Thompson and Pimentel, 1960). This property is also apparent from a group theoretical analysis. The stretching and bending modes belong to the A_1 and B_1 representations of the C_{2v} point group, respectively. The $B_1 \times B_1 = A_1$ symmetry of the first overtone is thus the same as that of the fundamental stretching mode, corresponding to the z polarisation, and differs from that of the fundamental bending transition. Furthermore, Thompson and Pimentel (1960) show that when the dipole moment function only depends on the distance between the hydrogen atom and the facing atom, the intensity of the fundamental stretching and bending overtone bands depends on the same charge mobility term, a term which is significantly enhanced by the formation of hydrogen bonds (e.g. Libowitzky and Rossman, 1997; Balan et al., 2008). Accordingly, it is suggested that the anomalously strong intensity of the bending overtone bands in the spectra of corundum-bearing divalent cations arises from the more significant H-bonding of OH groups compared with that of OH groups associated with Al vacancies and leading to the "3309 cm^{-1} series". In addition, a dominance of the longitudinal component of the dipole moment function in the intensity of overtone bands would also explain why their polarisation is similar to those determined for the fundamental OH stretching bands (Fukatsu et al., 2003; Jol-

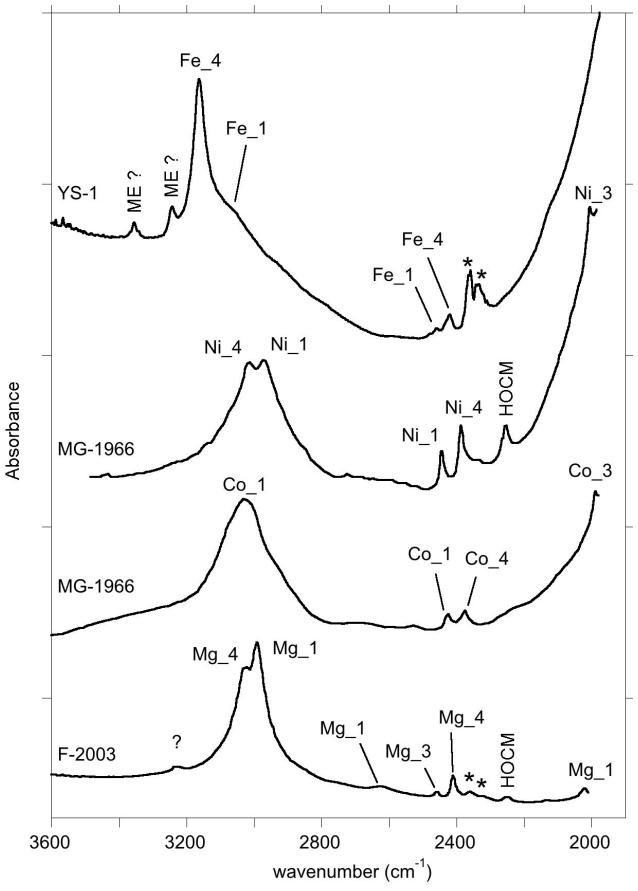

Figure 10. Summary of the assignment of the main FTIR bands of corundum-bearing divalent cations. The spectra are room temperature spectra of YS-1 sample, Ni- and Co-doped samples (MG-1966) from Müller and Günthard (1966), and Mg-doped sample (F-2003) from Fukatsu et al. (2003). HOCM: higher-order overtone of coupled mode (see text); ME: multiple excitation (anharmonic resonance or combination band involving the strong OH stretching excitation). The asterisks denote artefactual bands related to atmospheric CO_2.

lands and Balan, 2022). Note however that the OH defects in corundum display a lower symmetry (Fig. 1). In this case, transverse terms in the dipole moment function, as well as the anharmonicity of the potential, can affect the overtone intensity, which complicates the picture.

It is likely that the proposed mechanism also contributes to the enhancement of the two-phonon OH bending bands in the spectra of diaspore and groutite (Kohler et al., 1997). This mechanism differs from the enhancement of overtones by Fermi resonances, i.e. the anharmonic interaction between a fundamental transition and an overtone of a lower-frequency mode when both occur at a similar frequency. An anharmonic interaction between the bending overtone and the fundamental OH stretching excitations is however suggested by the broadening of the overtone bands observed above 2500 cm^{-1}.

4 Conclusions

In this study, hydrous defects in corundum associated with divalent cations have been investigated by theoretical modelling and experimentation in order to discuss the origin of bands frequently observed between 2000 and 3500 cm^{-1} in the FTIR spectra of natural, treated and synthetic corundum (Table 4). The series of bands observed below 2700 cm^{-1} in the spectra of samples containing Be, Mg, Co or Ni most likely correspond to overtone bands of OH bending modes. These overtone bands are likely enhanced by the electrical anharmonicity of the OH group involved in medium-strength hydrogen bonding. Most of these bands are significantly narrower than the corresponding OH stretching bands. They could therefore be efficiently used to identify specific configurations of hydrous defects in natural and synthetic corundum samples when OH stretching bands are broad and overlapping. This could be useful for gemological applications. More generally, the analytical importance of narrower bending infrared bands for the study of hydrogen-bonded systems has been pointed out by Novak (1974). In addition, the comparison of theoretical and experimental frequencies supports the assignment of the main bands observed in corundum samples containing divalent cations to specific defect configurations (Table 4, Fig. 10). The results support the assignment of the 3161 cm^{-1} band frequently observed in natural sapphire samples to structural OH groups associated with Fe^{2+} ions.

Code availability. PWscf and PHonon codes (Giannozzi et al., 2009) are available at https://www.quantum-espresso.org/ (last access: 6 October 2023). The pseudopotentials (Schlipf and Gygi, 2015) are available at http://www.quantum-simulation.org/potentials/sg15_oncv/ (last access: 6 October 2023). Structure drawings have been done using VESTA software (https://jp-minerals.org/vesta/en/, last access: 6 October 2023, Momma and Izumi, 2011).

Data availability. Theoretical structure and vibrational modes of the investigated models and experimental FTIR spectra of corundum samples from the GIA database are reported in the Supplement.

Supplement. The supplement related to this article is available online at: https://doi.org/10.5194/ejm-35-873-2023-supplement.

Author contributions. MCJ and EB initiated the study. EB performed the calculations. MCJ, SJ, MC, MG, KB and PG performed the experimental measurements and analysis. All co-authors contributed to the discussion of the results and preparation of the manuscript.

Competing interests. At least one of the (co-)authors is a member of the editorial board of *European Journal of Mineralogy*. The peer-review process was guided by an independent editor, and the authors also have no other competing interests to declare.

Disclaimer. Publisher's note: Copernicus Publications remains neutral with regard to jurisdictional claims in published maps and institutional affiliations.

Special issue statement. This article is part of the special issue "Probing the Earth: spectroscopic methods applied to mineralogy". It is not associated with a conference.

Acknowledgements. Calculations were performed using the HPC resources of the SACADO MeSU platform at Sorbonne Université and the HPC resources of IDRIS under allocation 2022-AD010910820R1 attributed by GENCI (Grand Équipement National de Calcul Intensif). The "Plateforme de spectroscopie" (IMPMC) and Noémie Brossut and Paul Lasserre (UFR TEB, Sorbonne Université) are thanked for their support in the experimental measurements. The "Collection de Minéraux" (IMPMC, Sorbonne Université) is thanked for providing us with the yellow sapphire sample. Pamela Cevallos and Tyler Smith (Gemological Institute of America) are thanked for introductions to the different types of spectrum observed in gemological analyses. We thank Boriana Mihailova and the two anonymous reviewers for their detailed and constructive comments.

Review statement. This paper was edited by Reto Gieré and Boriana Mihailova and reviewed by two anonymous referees.

References

Atikarnsakul, U. and Emmett, J. L.: Heat treatment effects on the behavior of the 3161 cm^{-1} feature in low-iron metamorphic yellow sapphire, Gems Gemol., 57, 286–288, 2021.

Balan, E.: Theoretical infrared spectra of OH defects in corundum (α-Al_2O_3), Eur. J. Miner., 32, 457–467, https://doi.org/10.5194/ejm-32-457-2020, 2020.

Balan, E., Lazzeri, M., Delattre, S., Meheut, M., Refson, K., and Winkler, B.: Anharmonicity of inner-OH stretching modes in hydrous phyllosilicates: assessment from first-principles frozen-phonon calculations, Phys. Chem. Minerals, 34, 621–625, https://doi.org/10.1007/s00269-007-0176-4, 2007.

Balan, E., Refson, K., Blanchard, M., Delattre, S., Lazzeri, M., Ingrin, J., Mauri, F., Wright, K., and Winkler, B.: Theoretical infrared absorption coefficient of OH groups in minerals, Am. Mineral., 93, 950–953, https://doi.org/10.2138/am.2008.2889, 2008.

Balmer, W. A., Leelawatanasuk, T., Atichat, W., Wathanakul, P., and Somboon, C.: Update on characteristics of heated yellow sapphires, Poster, Proceedings of the 1st International Gem and Jewelry Conference, 2006.

Balmer, W. A. and Krzemnicki, M. S.: Be-detection by FTIR on Corundum: A Preliminary Report, International Gemmological Conference, Vilnius, Lithuania, Abstracts Book, 69–71, 2015.

Baroni, S., de Gironcoli, S., Dal Corso, A., and Giannozzi, P.: Phonons and related crystal properties from density-functional perturbation theory, Rev. Mod. Phys., 73, 515–561, https://doi.org/10.1103/RevModPhys.73.515, 2001.

Beran, A.: Trace hydrogen in Verneuil-grown corundum and its colour varieties – an IR spectroscopic study, Eur. J. Mineral., 3, 971–975, https://doi.org/10.1127/ejm/3/6/0971, 1991.

Beran, A. and Rossman G. R.: OH in naturally occurring corundum, Eur. J. Mineral., 18, 441–447, https://doi.org/10.1127/0935-1221/2006/0018-0441, 2006.

Blum, H., Frey, R., Günthard, H. H., and Ha, T.K.: Ab initio SCF study of OHO^{3-} system and its relation to the structure of α-Al_2O_3:OHO^{3-} (Me^{2+}), Chem. Phys., 2, 262–270, https://doi.org/10.1016/0301-0104(73)80030-8, 1973.

Bonnet, M. and Fritsch, E.: Bandes d'absorption peu connues dans les spectres infrarouges du corindon: que signifient-elles, Gemmol. Francoph., 1–3, 2021.

Choudhary, G. and Vijay, S.: 3161 cm^{-1} infra-red feature in synthetic sapphires, GIA International Gemological Symposium, 2018.

Delattre, S., Balan, E., Lazzeri, M., Blanchard, M., Guillaumet, M., Beyssac, O., Haussühl, E., Winkler, B., Salje, E. K. H., and Calas, G.: Experimental and theoretical study of the vibrational properties of diaspore (α-AlOOH), Phys. Chem. Minerals, 39, 93–102, https://doi.org/10.1007/s00269-011-0464-x, 2012.

Eigenmann, K. and Günthard, H. H.: Hydrogen incorporation in doped α-Al_2O_3 by high temperature redox reactions, Chem. Phys. Lett., 12, 12–15, https://doi.org/10.1016/0009-2614(71)80605-X, 1971.

Fukatsu, N., Kurita, N., Oka, Y., and Yamamoto, S.: Incorporation of hydrogen into magnesium-doped α-alumina, Sol. State Ion., 162, 147–159, https://doi.org/10.1016/S0167-2738(03)00218-2, 2003.

Futazuka, T., Ishikawa, R., Shibata, N., and Ikuhara, Y.: First-principles calculations of group IIA and group IV impurities in α-Al_2O_3, Phys. Rev. Mater. 4, 073602, https://doi.org/10.1103/PhysRevMaterials.4.073602, 2020.

Ghosez, Ph., Michenaud, J. P., and Gonze, X.: Dynamical atomic charges: The case of ABO_3 compounds, Phys. Rev. B, 58, 6224–6240, https://doi.org/10.1103/PhysRevB.58.6224, 1998.

Giannozzi, P., Baroni, S., Bonini, N., Calandra, M., Car, R., Cavazzoni, C., Ceresoli, D., Chiarotti, G. L., Cococcioni, M., Dabo, I., Dal Corso, A., de Gironcoli, S., Fabris, S., Fratesi, G., Gebauer, R., Gerstmann, U., Gougoussis, C., Kokalj, A., Lazzeri, M., Martin-Samos, L., Marzari, N., Mauri, F., Mazzarello, R., Paolini, S., Pasquarello, A., Paulatto, L., Sbraccia, C., Scandolo, S., Sclauzero, G., Seitsonen, A. P., Smogunov, A., Umari, P., and Wentzcovitch, R. M.: Quantum ESPRESSO: a modular and open-source software project for quantum simulations of materials, [code], J. Phys. Cond. Mat., 21, 395502, https://doi.org/10.1088/0953-8984/21/39/395502, 2009.

Gonze, X. and Lee, C.: Dynamical matrices, Born effective charges, dielectric permittivity tensors, and interatomic force constants from density-functional perturbation theory, Phys. Rev. B, 55, 10355–10368, https://doi.org/10.1103/PhysRevB.55.10355, 1997.

Hamann, D. R.: Optimized norm-conserving Vanderbilt pseudopotentials, Phys. Rev. B, 88, 085117, https://doi.org/10.1103/PhysRevB.88.085117, 2013.

Hauffe, K. and Hoeffgen, D.: Zum mechanismus der umladung von kobaltionen im saphir, Berichte der Bunsengesellschaft für physikalische Chemie, 74, 537–546, 1970.

Hummel, G.: Etude en spectroscopie infrarouge d'une collections de saphirs jaunes à oranges, Diplome d'Université de Gemmologie, Université de Nantes, 2019.

Jollands, M. C., Blanchard, M., and Balan, E.: Structure and theoretical infrared spectra of OH defects in quartz, Eur. J. Mineral., 32, 311–323, https://doi.org/10.5194/ejm-32-311-2020, 2020.

Jollands, M. C. and Balan, E.: Beryllium incorporation in corundum, Mineral. Mag., 86, 758–766, https://doi.org/10.1180/mgm.2022.63, 2022.

Kohler, T., Armbruster, T., and Libowitzky, E.: Hydrogen bonding and Jahn-Teller distortion in groutite, α-MnOOH, and manganite, γ-MnOOH, and their relations to the manganese dioxides ramsdellite and pyrolusite, J. Sol. State Chem., 133, 486–500, https://doi.org/10.1006/jssc.1997.7516, 1997.

Libowitzky, E. and Rossman, G. R.: An IR absorption calibration for water in minerals, Am. Mineral., 82, 1111–1115, https://doi.org/10.2138/am-1997-11-1208, 1997.

Libowitzky, E. and Beran, A.: The structure of hydrous species in nominally anhydrous minerals: Information from polarized IR spectroscopy, Rev. Mineral. Geochem., 62, 29–52, https://doi.org/10.2138/rmg.2006.62.2, 2006.

Momma, K. and Izumi, F.: VESTA 3 for three-dimensional visualization of crystal, volumetric and morphology data, [code], J. Appl. Crystallogr., 44, 1272–1276, https://doi.org/10.1107/S0021889811038970, 2011.

Moon, A. R. and Phillips, M. R.: Defect clustering in H,Ti: α-Al_2O_3, J. Phys. Chem. Sol., 52, 1087–1099, https://doi.org/10.1016/0022-3697(91)90042-X, 1991.

Moon, A. R. and Phillips, M. R.: Defect clustering and color in Fe,Ti: α-Al_2O_3, J. Amer. Ceram. Soc., 77, 356–367, https://doi.org/10.1111/j.1151-2916.1994.tb07003.x, 1994.

Müller, R. and Günthard, H. H.: Spectroscopic study of the reduction of nickel and cobalt ions in sapphire, J. Chem. Phys., 44, 365–373, https://doi.org/10.1063/1.1726471, 1966.

Nibbering, E. T., Dreyer, J., Kühn, O., Bredenbeck, J., Hamm, P., and Elsaesser, T.: Vibrational dynamics of hydrogen bonds, in: Analysis and Control of Ultrafast Photoinduced Reactions, edited by: Kühn, O. and Wöste, L., Chem. Phys., 87, Springer, Berlin, Heidelberg, https://doi.org/10.1007/978-3-540-68038-3_7, 2007.

Nibler, J. W. and Pimentel, G. C.: Infrared spectra of Cesium bihalide salts, J. Chem. Phys., 47, 710, https://doi.org/10.1063/1.1711944, 1967.

Novak, A.: Hydrogen bonding in solids. Correlation of spectroscopic and crystallographic data, in: Large Molecules, Struct. Bond., Springer, Berlin, Heidelberg, 18, https://doi.org/10.1007/BFb0116438, 1974.

Perdew, J. P., Burke, K., and Ernzerhof, M.: Generalized Gradient Approximation Made Simple, Phys. Rev. Lett., 77, 3865–3868, https://doi.org/10.1103/PhysRevLett.77.3865, 1996.

Ramírez, R., González, R., Colera, I., and Vila, R.: Protons and deuterons in magnesium-doped sapphire crystals, J. Am. Ceram. Soc., 80, 847–850, https://doi.org/10.1111/j.1151-2916.1997.tb02913.x, 1997.

Ramírez, R., Colera, I., González, R., Chen, Y., and Kokta, M. R.: Hydrogen-isotope transport induced by an electric field in α-Al_2O_3 single crystals, Phys. Rev. B, 69, 014302, https://doi.org/10.1103/PhysRevB.69.014302, 2004.

Rossi, M., Biondi, R., Rizzi, R., Corriero, N., Sequino, F., and Vergara, A.: Mechanism of Be-Thermodiffusion in Rutile Inclusions of Fancy Sapphires, Cryst. Growth Design, 22, 6493–6503, https://doi.org/10.1021/acs.cgd.2c00700, 2022.

Ryskin, Y. A. I.: The vibrations of protons in minerals: hydroxyl, water and ammonium, in: The Infrared Spectra of Minerals, edited by: Farmer, V. C., Mineral. Soc., 137–181, 1974.

Sangsawong, S., Pardieu, V., Raynaud, V., and Engniwat, S.: "Punsiri" type FTIR spectral features in natural yellow sapphires, Gems Gemol., 52, 325–327, 2016.

Schlipf, M. and Gygi, F.: Optimization algorithm for the generation of ONCV pseudopotentials, [code], Comput. Phys. Comm., 196, 36, https://doi.org/10.1016/j.cpc.2015.05.011, 2015.

Schwarz, D., Pardieu, V., Saul, J.M., Schmetzer, K., Laurs, B.M., Giuliani, G., Klemm, L., Malsy, A.-K., Erel, E., Hauzenberger, C., Du Toit, G., Fallick, A. E., and Ohnenstetter, D.: Rubies and Sapphires from Winza, Central Tanzania, Gems Gemol., 44, 322–347, 2008.

Smith, C. P. and Van der Bogert, C.: Infrared spectra of gem corundum, Gems Gemol., 42, 92–93, 2006.

Soonthorntantikul, W., Khowpong, C., Atikarnsakul, U., Saeseaw, S., Sangsawong, S., Vertriest, W., and Palke, A.: Observations on the heat treatment of basalt-related blue sapphires, Gemological Institute of America Report, 60 pp., 2019.

Stegmann, C., Vivien, D., and Mazières, C.: Etude des mode de vibration des oxyhydroxydes d'aluminium boehmite et diaspore, Spectrochim. Acta, 29A, 1653–1663, 1973.

Thompson, W. E. and Pimentel, G. C.: The first overtone of the hydrogen bending mode of chloroform: Enhancement by hydrogen bonding, Z. Elektrochem., 64, 748–753, https://doi.org/10.1002/bbpc.196000040, 1960.

T-Thienprasert, J., Boonchun, A., Reunchan, P., and Limpijumnong, S.: Identification of hydrogen defects in α-Al_2O_3 by first-principles local vibration mode calculations, Phys. Rev. B, 95, 134103, https://doi.org/10.1103/PhysRevB.95.134103, 2017.

Volynets, F. K., Sidorova, Y. A., and Stsepuro, N. A.: OH-groups in corundum crystals grown by the Verneuil technique, J. Appl. Spectr., 17, 1088–1091, 1972.

Zhang, G., Lu, Y., and Wang, X.: Hydrogen interactions with intrinsic point defects in hydrogen permeation barrier of α-Al_2O_3: a first-principles study, Phys. Chem. Chem. Phys., 16, 17523, https://doi.org/10.1039/c4cp01382d, 2014.